

11-21-2005

Vorticity-Based Detection of Tropical Cyclogenesis

Michelle Marie Hite
Florida State University

Follow this and additional works at: <http://diginole.lib.fsu.edu/etd>

Recommended Citation

Hite, Michelle Marie, "Vorticity-Based Detection of Tropical Cyclogenesis" (2005). *Electronic Theses, Treatises and Dissertations*. Paper 4027.

THE FLORIDA STATE UNIVERSITY
COLLEGE OF ARTS AND SCIENCES

VORTICITY-BASED DETECTION OF TROPICAL CYCLOGENESIS

By

MICHELLE M. HITE

A Thesis submitted to the
Department of Meteorology
in partial fulfillment of the
requirements for the degree of
Master of Science

Degree Awarded:
Spring Semester, 2006

The members of the Committee approve the thesis of Michelle M. Hite defended on November 22, 2005.

James J. O'Brien
Professor Directing Thesis

Mark A. Bourassa
Committee Member

Paul D. Reasor
Committee Member

The Office of Graduate Studies has verified and approved the above named committee members.

This thesis is dedicated to my grandfather, Fred Bostian, who inspired me to pursue Meteorology. I hope all your dreams came true through me.

ACKNOWLEDGEMENTS

The base funding for this project came from NOAA CDEP. Additional support came from the NASA/OSU SeaWinds project and the NASA OVWST project. QuikSCAT data are produced by Remote Sensing Systems and sponsored by the NASA OVWST. Data are available at www.remss.com.

I would like to acknowledge and thank my major professor Dr. James J. O'Brien for all his advice and guidance. I would also like to thank Dr. Mark Bourassa for his assistance and guidance through this project, along with my other committee member, Dr. Paul Reasor.

I would like to especially thank all of those at COAPS for any advice or assistance.

I would like to thank my family for all of their support as I pursue all of my goals. Much appreciation goes to my sister, Jennifer Hite, for all of her reviews and critiques of my thesis.

Also, I would like to thank my fiancé, Tony Gierach, for his unending support, all of his assistance in helping me obtain my Master's degree, and all of the times he listened to my thesis so that I could perfect it. I am grateful for his support and assistance.

TABLE OF CONTENTS

List of Figures	vii
Abstract	ix
1. INTRODUCTION	1
2. BACKGROUND	4
2.1 Principles of Scatterometry.....	4
2.2 The SeaWinds Scatterometer.....	5
3. DATA	8
3.1 Scatterometer Data.....	8
3.2 GOES Imagery.....	8
4. METHODOLOGY	10
4.1 Detection Technique	10
4.2 Threshold Determination	11
4.3 Track Assessment	12
5. RESULTS	14
5.1 Isabel (2003)	17
5.2 Debby (2000)	22
6. DISCUSSIONS.....	27
6.1 The Initial Stage.....	28
6.2 The Intermediate Stage	29
6.3 The Near-TC Stage	29
6.4 Pre-TC Track Transition	30
6.5 Future Improvements	30
7. CONCLUSIONS.....	32

REFERENCES	33
BIOGRAPHICAL SKETCH	36

LIST OF FIGURES

Figure 1: The spacecraft and antenna geometries for SeaWinds. Outer beam is v-pol and inner beam is h-pol (adapted from Weissman et al. 2003)	6
Figure 2: Probability of Detection (POD) graph. Lower threshold values result in a higher probability of detection and increased false alarms. Higher threshold values result in detection of stronger systems (more misses) and, hence, less false alarms	12
Figure 3: Examples of the early stages of TCG that are identified by the vorticity-based detection technique. (a) Floyd, 46 hours before classification as a tropical depression. The vorticity signature shown is associated with the easterly wave that spawned Floyd. (b) Nicholas, 64 hours before classification as a tropical depression. The vorticity signature shown is associated with the easterly wave that produced Nicholas. (c) Michael, 38 hours before classification as a subtropical depression. The vorticity signature shown is associated with the upper-level cold low that interacted with a stationary front to create Michael. (d) Noel, 26 hours before classification as a subtropical storm. The vorticity signature shown is associated with the non-tropical occluded low that spawned Noel. Each example illustrates an apparent surface circulation	16
Figure 4: GOES infrared images associated with pre-TC Isabel (2003) for (a) 1 September at 1745 UTC, (b) 2 September at 845 UTC, (c) 3 September at 845 UTC, (d) 3 September at 2045 UTC, (e) 4 September at 2045 UTC, (f) 5 September at 845 UTC, and (g) 5 September at 2045 UTC (courtesy NOAA/NESDIS/CLASS: www.class.noaa.gov)	18
Figure 5: QuikSCAT vorticity images associated with pre-TC Isabel (2003) and the corresponding tracking times. (a) 1 September at 1856 UTC, 101 hours. (b) 2 September at 739 UTC, 88 hours. (c) 3 September at 714 UTC, 65 hours. (d) 3 September at 1944 UTC, 52 hours. (e) 4 September at 1918 UTC, 29 hours. (f) 5	

September at 803 UTC, 16 hours. (g) 5 September at 2032 UTC, 3 hours	19
Figure 6: Track of the tropical disturbance associated with pre-TC Isabel (2003). Triangles represent the associated QuikSCAT images, and the number above or below each triangle signify the tracking time for that image. The number ‘0’ represents when the NHC classified Isabel as a tropical depression	21
Figure 7: GOES infrared images associated with pre-TC Debby (2000) for (a) 15 August at 2045 UTC, (b) 16 August at 845 UTC, (c) 16 August at 2045 UTC, (d) 17 August at 2045 UTC, (e) 18 August at 845 UTC, (f) 18 August at 2045 UTC, and (g) 19 August at 845 UTC (courtesy NOAA/NESDIS/CLASS)	23
Figure 8: QuikSCAT vorticity images associated with pre-TC Debby (2000) and the corresponding tracking times. (a) 15 August at 1859 UTC, 95 hours. (b) 16 August at 742 UTC, 82 hours. (c) 16 August at 2014 UTC, 70 hours. (d) 17 August at 1950 UTC, 46 hours. (e) 18 August at 833 UTC, 33 hours. (f) 18 August at 2104 UTC, 21 hours. (g) 19 August at 808 UTC, 10 hours	24
Figure 9: Track of the tropical disturbance associated with pre-TC Debby (2000). Triangles represent the associated QuikSCAT images, and the number above each triangle signifies the tracking time for that image. The number ‘0’ represents when the NHC classified Debby as a tropical depression	26

ABSTRACT

Ocean wind vectors from the SeaWinds scatterometer on QuikSCAT and GOES imagery are used to develop an objective technique that can detect and monitor tropical disturbances associated with the early stages of tropical cyclogenesis in the Atlantic basin. The technique is based on identification of surface vorticity and wind speed signatures that exceed certain threshold magnitudes, with vorticity averaged over an appropriate spatial scale. The threshold values applied herein are determined from the precursors of 15 tropical cyclones during the 1999-2004 Atlantic hurricane seasons using research-quality QuikSCAT data. Tropical disturbances are found for these cases within a range of 19 hours to 101 hours before classification as tropical cyclones by the National Hurricane Center (NHC).

The 15 cases are further subdivided based upon their origination source (i.e., easterly wave, upper-level cut-off low, stagnant frontal zone, etc). Primary focus centers on the cases associated with tropical waves, since these waves account for approximately 63% of all Atlantic tropical cyclones. The detection technique illustrates the ability to track these tropical disturbances from near the coast of Africa. Analysis of the pre-tropical cyclone (TC) tracks for these cases depict stages, related to wind speed and precipitation, in the evolution of an easterly wave to tropical cyclone.

1. INTRODUCTION

Tropical cyclogenesis (TCG), although an already well researched area, remains a highly debatable and unresolved field. While considerable attention has been paid to tropical cyclone formation, little attention has focused on observational studies of the very early stages of TCG, otherwise referred to as the genesis stage. In the past, the early stages of TCG were unverifiable in surface observations, due to the paucity of meteorological data over the tropical oceans. The advent of wide swath scatterometers helped alleviate this issue by affording the scientific community with widespread observational surface data across the tropical basins. One such instrument is the SeaWinds scatterometer, aboard the QuikSCAT satellite, which infers surface wind speed and direction. Launched in 1999, this scatterometer has encouraged various studies regarding early identification of tropical disturbances (Liu et al. 2001; Katsaros et al. 2001; Sharp et al. 2002). These studies, though operational in intent, hypothesized the potential for SeaWinds data to be applied towards research applications (i.e., genesis stage research). The main goal of this study is to develop an objective technique that will detect the early stages of TCG in the Atlantic basin using SeaWinds data.

Liu et al. (2001), Katsaros et al. (2001), and Sharp et al. (2002) demonstrated the ability to identify tropical disturbances, discrete weather systems of apparently organized convection that maintain their identity for 24 hours or more and are too weak to be classified as tropical cyclones (i.e., tropical depressions, tropical storms, or hurricanes) by the National Hurricane Center (NHC). Each technique utilized surface wind data obtained by the SeaWinds scatterometer. However, the criteria that defined their identification method differed. Sharp et al. (2002) employed vorticity as his detection condition, whereas, Liu et al. (2001) and Katsaros et al. (2001) relied upon closed circulations apparent in the scatterometer data. Using a threshold of vorticity over a defined area, Sharp et al. (2002) identified numerous tropical disturbances and assessed whether or not they were likely to develop into tropical cyclones. Detection was based on surface structure, requiring sufficiently strong vorticity averaged over a large surface area. Unlike Sharp et al. (2002), Katsaros et al. (2001) and Liu et al. (2001) concentrated on disturbances that would develop into classified tropical cyclones. They examined

surface wind patterns and looked for areas of closed circulation, successfully detecting tropical disturbances before designation as depressions. These studies illustrated the usefulness of SeaWinds data towards tropical disturbance detection, with the intent of improving operational activities. The early identification of surface circulations presented in these studies suggests an opportunity to detect the early stages of TCG, setting the basis for this paper.

The detection technique described herein has the potential for applications in the scientific and operational communities. In operational applications, the forecasting community can implement the detection technique as an additional observational tool. In doing so, the technique can enhance the current observing system employed to identify and monitor tropical weather systems, thereby reducing the time forecasters spend examining the tropics for incipient systems. In research applications, identification of the early stages of TCG can enhance understanding in regions where little research has been conducted due to the prior inability to conclusively locate tropical disturbances. This study focuses on the Atlantic basin, but the detection technique can be applied to other tropical regions, such as the Pacific basin, after adjusting the threshold values to account for regional differences in TCG mechanisms.

The ability to detect the early stages of tropical cyclogenesis provides an opportunity to classify tropical disturbances in the Atlantic basin based on the source of initial cyclonic vorticity maximum. Following categorization by Bracken and Bosart (2000) these sources include disturbances associated with: (i) monsoon troughs or the intertropical convergence zone (Riehl 1954, 1979), (ii) an easterly wave (Carlson 1969; Burpee 1972, 1974, 1975; Reed et al. 1977; Thorncroft and Hoskins 1994 ab), (iii) a stagnant frontal zone originating in the midlatitudes (Frank 1988; Davis and Bosart 2001), (iv) mesoscale convective systems (MCSs; Bosart and Sanders 1981; Ritchie and Holland 1997; Simpson et al. 1997; Bister and Emanuel 1997; Montgomery and Enagonio 1998), and (v) upper-level cut-off lows that penetrate to lower levels (Avila and Rappaport 1996). Among these, our research in the Atlantic basin affords the possibility to investigate cases associated with easterly waves. Of great interest is the prospect to examine the connection between a cold-core wave disturbance in the tropical easterlies and a warm-core tropical cyclone, which remains an unresolved issue in TCG research.

Easterly waves are of great importance since approximately 63% of tropical cyclones in the Atlantic basin originate from African easterly waves (Avila and Pasch 1992).

Another fundamental issue with tropical cyclone genesis involves the development of surface circulations during the pre-WISHE (Wind Induced Surface Heat Exchange) stage (P. D. Reasor 2005, personal communication). The fine details of the pre-WISHE process cannot be resolved with SeaWinds data. However, SeaWinds data does allow for an observationally-based estimate of vorticity available at the surface prior to the pre-WISHE stage, which is needed for numerical model initializations.

The outline for this paper is as follows. Background information regarding the basic principles of scatterometry and the SeaWinds scatterometer is presented in section 2. In section 3, the scatterometer data and GOES imagery employed in this study are detailed. The methodology behind the vorticity-based detection technique, including determination of threshold values and track assessment is described in section 4. Results of the detection technique are presented in section 5, with subsections dedicated to two individual case studies. The influence of rain on QuikSCAT winds are discussed and related to the evolution of wind and rain rates in tropical disturbances in section 6. Finally, conclusions are summarized in section 7. Overall, the detection technique proves very effective, identifying tropical disturbances associated with the early stages of tropical cyclogenesis approximately 19 hours to 101 hours before classification as tropical cyclones by the NHC.

2. BACKGROUND

2.1 Principles of Scatterometry

Scatterometers emit microwave pulses to the ocean surface and measure the backscattered power in the return echo. Microwaves are scattered by small-scale water waves (i.e., capillary waves), which are in near equilibrium with the wind. As a result, capillary waves react quickly to surface wind changes (i.e., wind speed and direction). Modulation of the waves alters the surface roughness of the ocean, affecting the radar cross section and, hence, the magnitude of backscattered power received by the instrument. From the backscattered power, the normalized radar cross section (σ^o) is obtained by inverting the radar equation (Naderi et al. 1991).

Scatterometers provide multiple measurements of σ^o at various azimuth angles. These measurements are organized into square bins called wind vector cells (WVCs). The method that estimates the wind velocity associated with σ^o measurements is the wind retrieval process.

The first step of the wind retrieval process is wind inversion. Wind inversion determines the scatterometer wind solutions that minimize an objective function, which measures the squared difference between observed and modeled backscatter (σ^o). Due to near symmetry, the objective function typically has several local minima. The wind solutions associated with these minima are otherwise referred to as ambiguities or aliases. These aliases are sorted according to rank, where rank one corresponds to the solution that has the lowest objective function value, rank two to the solution that has the next lowest objective function value, etc (Naderi et al. 1991). The modeled backscatter (σ^o) is determined by the geophysical model function (GMF).

The GMF is an empirical nonlinear model that describes the relationship between wind velocity and σ^o . This function is written as:

$$\sigma^o = F(u, \chi, \theta, \text{pol}, f) \quad (1)$$

where u is the wind speed, χ is the relative direction (the angle between the wind direction and the look direction of the scatterometer), θ is the surface incidence angle, pol is the electromagnetic polarization, and f is the radar frequency (Naderi et al. 1991).

Other factors such as temperature, ocean salinity, and foam also affect the relationship between wind and σ^o , but they are assumed to be small and considered noise in the geophysical model function (Richards 1999).

After wind inversion, the second step of the wind retrieval process is an ambiguity removal algorithm. Due to noise and the multiple wind solutions (i.e., ambiguities) that result from wind inversion, this step is often necessary to yield a unique wind vector solution. Correct ambiguity removal results in selection of the ambiguity that is closest to the actual wind vector (Naderi et al. 1991). Unfortunately, ambiguity removal algorithms are prone to errors (section 2.2).

2.2 The SeaWinds Scatterometer

The QuikSCAT satellite was launched on June 19, 1999 as a “quick recovery” mission to fill the gap created by the loss of data from the NASA scatterometer (NSCAT) when the ADEOS satellite lost power in June 1997. It orbits the earth sun-synchronously, with an orbital height of approximately 800 km above the equator. The orbital and recurrent periods of the QuikSCAT satellite are 101 minutes and 4 days, respectively. QuikSCAT swaths are 1800 km wide and cover over 90% of the earth’s surface in 24 hours.

The measuring instrument aboard the QuikSCAT satellite is the SeaWinds scatterometer. It is an active microwave sensor that uses a rotating dish antenna with two conically rotating pencil beams to acquire multiple measurements of backscattered power from different viewing geometries, which are then organized into 25x25 km WVCs. Herein a horizontally polarized (h-pol) beam at an incidence angle of 46.25 $^\circ$ and a vertically polarized (v-pol) beam at an incidence angle of 54 $^\circ$ trace the surface of the earth in a helical pattern, receiving backscatter measurements fore and aft the orbiting satellite (Figure 1). The measurement geometry that results from this scanning beam configuration varies across the swath. At swath edges there is very little azimuth variation between the fore and aft beams and measurements taken are only vertically polarized; whereas, the azimuth difference between the fore and aft beams is approximately 180 $^\circ$ in the nadir region and measurements taken are both vertically and

horizontally polarized. However, the measurements in the nadir region are nearly identical as a result of symmetry in the GMF. Therefore, poor viewing geometries for wind retrieval occur in the nadir region and at swath edges. The optimal region for wind retrieval is in the mid-swath, which is also known as the “sweet spot.” The mid-swath is approximately 200-700 km on either side of the satellite track.

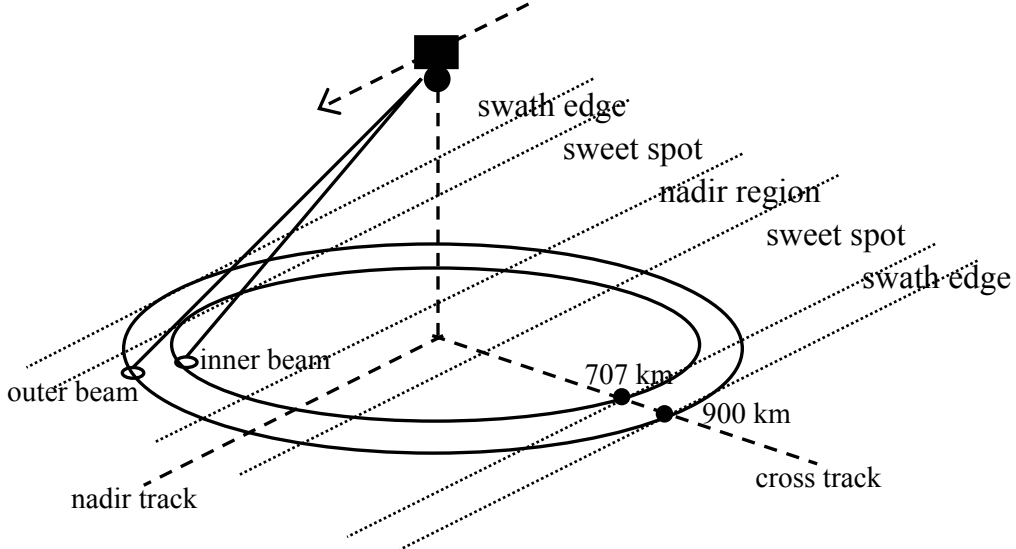


Figure 1: The spacecraft and antenna geometries for SeaWinds. Outer beam is v-pol and inner beam is h-pol (adapted from Weissman et al. 2003).

The ambiguity removal algorithm used by QuikSCAT is a vector median filter (Shaffer et al. 1991). This filter is initialized with the ambiguity closest to the National Center for Environmental Prediction (NCEP) 2.5° wind fields (Wentz et al. 1999). Once initialized, the median filter repeatedly selects the alias at each WVC that is closest to the actual wind vector until convergence is attained. The shortcoming of this approach, however, is that it is only successful if a majority of the initial ambiguities correspond to the true wind (Shaffer et al. 1991). Since the selected winds are horizontally consistent, ambiguity removal errors tend to occur in patches or lines and are often approximate direction reversals (roughly 180°).

For SeaWinds, wind retrieval is problematic for several conditions. First, the wind retrieval process is ill-conditioned at the edges of swaths. At the edge, the median filter has fewer neighboring points to use. Second, wind retrieval is less accurate at low wind speeds ($< 4 \text{ ms}^{-1}$) due to a low signal-to-noise ratio (SNR; Donelan and Pierson

1987). At these speeds, parts of the ocean surface act more like smooth reflectors than scatterers. Third, rain can greatly influence backscatter observations. In the presence of rain, the characteristics of the scatterometer signal are distorted because of backscatter off the rain, attenuation of the signal passing through the rain (Weissman et al. 2002), and modification of the surface shape by raindrop impacts (Bliven et al. 1993; Sobieski et al. 1995; 1999). As a result, wind directions in rain-contaminated WVCs (where the rain signal is similar or greater in magnitude to the wind signal) are often cross-swath rather than the true direction.

3. DATA

Ocean wind vectors are obtained from the SeaWinds scatterometer for the Atlantic basin. QuikSCAT has slightly less than twice-daily coverage over this area and, hence, provides infrequent temporal sampling. To provide continuity of the track and verification of tropical disturbances between the relatively sparse QuikSCAT overpasses, GOES infrared images are acquired and compiled into animations. These animations allow cloud features that are associated with the surface vorticity signatures to be tracked. The conjunction of QuikSCAT and GOES is discussed in more detail in section 4.3.

3.1 Scatterometer Data

The scatterometer data that is used in this study is the simplified Ku2001 dataset produced by Florida State University's Center for Ocean-Atmospheric Prediction Studies (COAPS). It contains wind vectors, rain flags, locations, and times. The geophysical model function (GMF) used to obtain this data is the Ku2001 product developed by Remote Sensing Systems (RSS). The Ku2001 product is currently the most accurate GMF for most meteorological conditions (Bourassa et al. 2003). It performs far better near nadir, swath edges, and rain than either the science quality product from Jet Propulsion Laboratory (JPL) or the near real-time product from NOAA/NESDIS. This improved vector wind retrieval algorithm provides a fully integrated stand-alone rain flag and the capability to retrieve winds up to 70 m/s (Wentz et al. 2001). The scatterometer winds are calibrated to equivalent neutral winds at a height of 10 meters above the local mean water surface (Bourassa et al. 2003).

3.2 GOES Imagery

Geostationary Operational Environmental Satellites (GOES) circle the Earth in a geosynchronous orbit approximately 35,800 km above the Earth's equator. GOES-East is located at 75°W and GOES-West is located at 135°W. For our research, we utilize GOES-East due to its location over the Atlantic Ocean. The two GOES-East satellites

are GOES-8 (GOES-I) and GOES-12 (GOES-M). GOES-12 is the current satellite in operation, replacing GOES-8 on April 3, 2003. Both satellites have a three-axis, body-stabilized design, which provides significant improvements in weather imagery and atmospheric sounding information. They are equipped with a separate Imager and Sounder allowing simultaneous and independent imaging and sounding; however, we only focus on the Imager with an infrared resolution of approximately 4 km at nadir.

GOES-8 and GOES-12 infrared images are obtained from the NOAA/NESDIS Comprehensive Large Array-data Stewardship System (CLASS) for our 15 tropical cyclone cases during the 1999-2004 Atlantic hurricane seasons. Images are acquired approximately every three hours and compiled into separate animations, with a backward and forward-in-time progression.

4. METHODOLOGY

4.1 Detection Technique

The vorticity-based detection technique used in this study is a variation of the method developed by Sharp et al. (2002). This technique calculates relative vorticity within the SeaWinds swaths and applies a mean vorticity threshold over a specified spatial area (Sharp et al. 2002). Different criteria are utilized than those of Sharp et al. (2002), permitting identification of tropical disturbances prior to classification as tropical cyclones by the NHC.

The spatial scale for averaging vorticity within the SeaWinds swaths is a 100 km by 100 km area. Individual vorticity values are calculated from wind observations at the center of each grid cell, defined by 4 [2 x 2] adjacent scatterometer vectors, by determining the circulation around each box and then dividing through by the area (Sharp et al. 2002). This method enables the vorticity to be calculated at the same spatial density as the wind observations. In each calculation a minimum of 3 wind vectors out of the 4 in a square are required. The wind vector data we use in this approach includes rain-flagged data, which are prone to ambiguity removal errors (reversal of wind direction, section 2.2). Incorporation of rain-flagged data can affect the vorticity calculation, resulting in noise. How this noise compares to the signal varies across the QuikSCAT vorticity-based track of tropical disturbances and is discussed in section 6.

The criteria that define the detection technique consist of three components. The thresholds used in these components are greatly reduced as compared to those of Sharp et al. (2002). The criteria defined require that within the specified spatial scale (100 km by 100 km area) the average vorticity must exceed a minimum vorticity threshold, the maximum rain-free wind speed must exceed a minimum wind speed threshold, and that these conditions be met in at least 80% of the vorticity cells within 50 km of the vorticity points being tested. If these criteria are met then the system under consideration is deemed a tropical disturbance, which may develop into a tropical cyclone. For this study, the 15 tropical cyclone cases used will develop as a result of our initial selection.

4.2 Threshold Determination

The threshold values defined in our detection technique are determined using research-quality SeaWinds data for 15 tropical cyclones during the 1999-2004 Atlantic hurricane seasons. In preliminary examples we applied a speed and vorticity threshold of 4.0 ms^{-1} and $2.0 \times 10^{-5} \text{ s}^{-1}$, respectively. Results showed that 65 overpasses fit these criteria; however, some of the vorticity signatures identified were indistinguishable from noise (i.e., false alarms). Therefore, it was determined that these threshold values were too small. To reduce the number of false alarms found in our preliminary example, a categorical score is computed for a range of vorticity and wind speed thresholds to determine appropriate values.

The categorical score considered in this study is the probability of detection (POD), which evaluates the effectiveness of detection techniques. It is defined as:

$$POD = \frac{H}{H + M} \quad (2)$$

where H is the number of hits and M is the number of misses. In QuikSCAT overpasses, a “hit” is a vorticity signature that fulfills the detection technique’s criteria within close proximity (175 km) to its associated cloud cluster center, and a “miss” is a vorticity signal that does not meet the detection technique’s criteria within the vicinity of its corresponding cloud mass. The POD score measures the ability of our technique to accurately identify tropical disturbances in the correct locations. A score of 1 indicates perfect detection (all vorticity signatures in the QuikSCAT overpasses are hits), whereas, a score of zero represents negligible detection (all vorticity signatures in the QuikSCAT overpasses are misses).

In order to test this method, a POD plot is produced that assesses the contributions from both wind speed and vorticity thresholds in regards to our preliminary example (Figure 2). This plot illustrates that low threshold values result in a higher probability of detection (albeit more false alarms), whereas, high thresholds result in a lower probability of detection. A POD score of 1 is most desirable since it represents perfect detection; however, the test cases include two conditions that are indistinguishable from noise. Through analysis, the 96% POD contour is chosen based on its large gradient and high

sensitivity area, as well as its reduction of false alarms. Threshold values associated with this contour include a vorticity and wind speed threshold of $5.0 \times 10^{-5} \text{ s}^{-1}$ and 6.3 ms^{-1} , respectively. Utilization of these values within our detection technique shows that 62 overpasses meet our criteria.

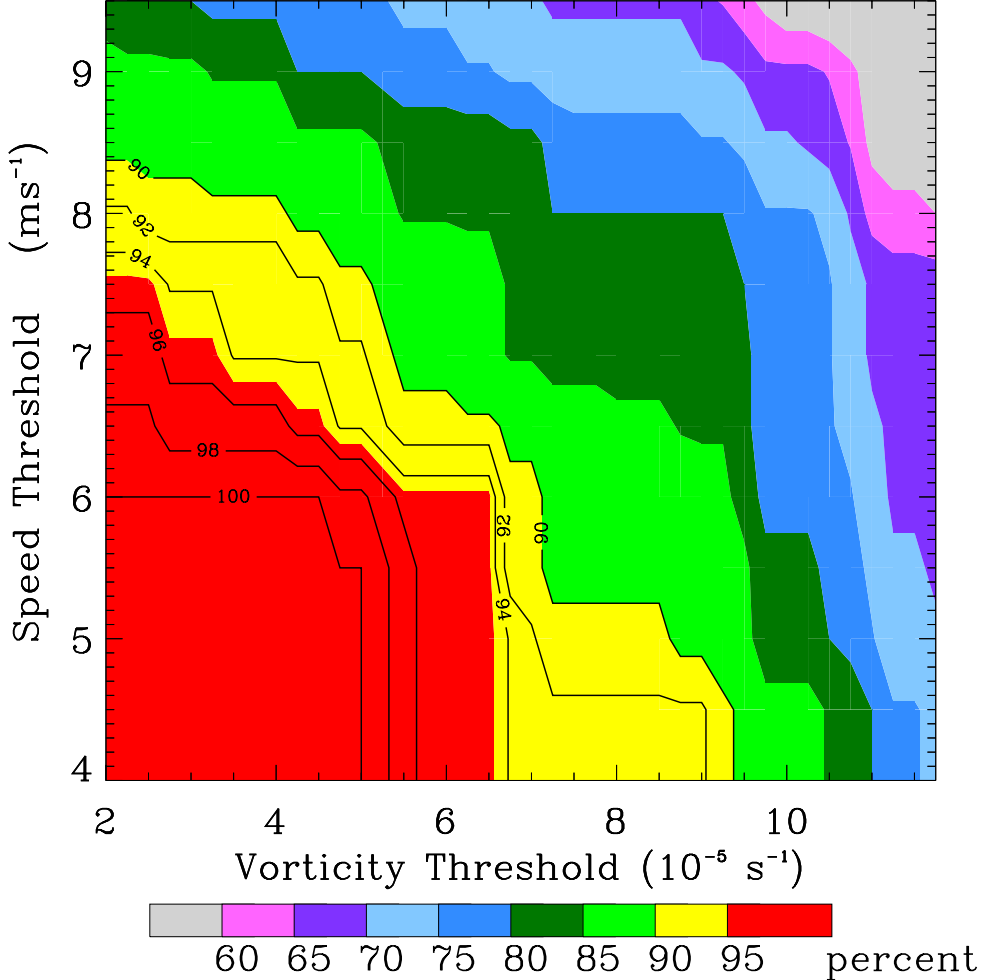


Figure 2: Probability of Detection (POD) graph. Lower threshold values result in a higher probability of detection and increased false alarms. Higher threshold values result in detection of stronger systems (more misses) and, hence, less false alarms.

4.3 Track Assessment

The combination of QuikSCAT's four-day repeat cycle and approximate twice-daily coverage (globally averaged) affords the Atlantic basin with infrequent temporal samplings, which proves problematic in regards to studies based purely on QuikSCAT. As previously mentioned, 62 QuikSCAT overpasses contain tropical disturbances that

fulfill the detection technique's criteria. Though substantial in number, the time period between these overpasses is anything but adequate, with a range from 11 to 36 hours. These temporal gaps may not be a problem for detection of existing tropical cyclones or tropical disturbances near classification; however, they are significant for identification of tropical disturbances associated with the early stages of TCG. Gaps between detection generate uncertainty regarding a tropical disturbance's track and positioning in time. To provide continuity of the track and validate the vorticity signatures identified by the detection technique, the combination of GOES and QuikSCAT is necessary.

GOES infrared images provide supplementary observational guidance between the relatively sparse QuikSCAT overpasses. For the 15 cases, GOES animations are created with a backward and forward-in-time progression. These animations allow the cloud mass associated with a tropical disturbance to be tracked, providing insight into the position and track extent of the tropical disturbance. For a large, organized cloud mass, the location of the corresponding QuikSCAT vorticity signature is evident. However, through the pre-tropical cyclone (TC) tracks of our 15 cases it is apparent that the cloud masses go through phases of intensification and de-intensification. Categorization of these phases is dependent upon spatial size, organization, and convective features. If the cloud mass associated with a tropical disturbance is going through de-intensification it may separate into numerous cloud clusters, making it difficult to pinpoint a specific cloud cluster and, hence, a position to use in the corresponding QuikSCAT overpass to identify a vorticity signature from surrounding signals. Therefore, the use of QuikSCAT and GOES together greatly reduces the ambiguity in determining which cloud system to track.

5. RESULTS

Results for the 15 tropical cyclones during the 1999-2004 Atlantic hurricane seasons are illustrated in Table 1. These systems are chosen because their coverage is adequate for reasonable study in the Atlantic basin. Ten of the 15 tropical cyclones originate as tropical waves off the coast of Africa (i.e., African easterly waves). These include Floyd (1999), Debby (2000), Nadine (2000), Jerry (2001), Dolly (2002), Danny (2003), Isabel (2003), Juan (2003), Nicholas (2003), and Alex (2004). The other five cases originate from sources other than tropical waves, such as upper-level cut-off lows and stagnant frontal zones. These include Florence (2000), Michael (2000), Karen (2001), Noel (2001), and Gustav (2002).

Table 1: Results for 15 tropical cyclones during the 1999-2004 Atlantic hurricane seasons. The last column signifies the hours elapsed between the NHC initial classification and our earliest tropical disturbance identification (i.e., tracking time).

Storm	Year	NHC Initial Classification	Tracking Time
Floyd	1999	Tropical Depression	46
Debby	2000	Tropical Depression	95
Florence	2000	Subtropical Depression	67
Michael	2000	Subtropical Depression	38
Nadine	2000	Tropical Depression	50
Jerry	2001	Tropical Depression	101
Karen	2001	Extratropical Low	19
Noel	2001	Subtropical Storm	62
Dolly	2002	Tropical Depression	53
Gustav	2002	Subtropical Depression	25
Danny	2003	Tropical Depression	38
Isabel	2003	Tropical Depression	101
Juan	2003	Tropical Depression	26
Nicholas	2003	Tropical Depression	64
Alex	2004	Tropical Depression	79

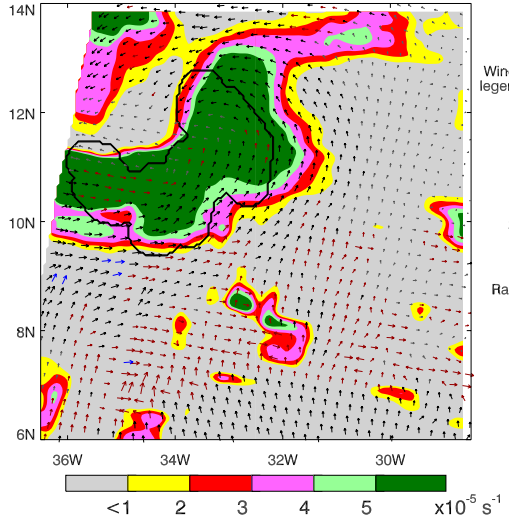
Tropical disturbances associated with the early stages of TCG are found for these cases within a range of 19 hours to 101 hours before classification as tropical cyclones by the NHC (Table 1). The average tracking time for these systems is approximately 58 hours, where tracking time is defined as the time elapsed between the NHC initial classification and our earliest tropical disturbance identification. Some examples of the technique in identifying the early stages of TCG are illustrated in Figures 3a-d. These

figures illustrate spatially averaged vorticity signatures that are overlaid with solid black contours, which signify the locations where the detection technique's criteria are met within 175 km from the point of convection in the associated GOES infrared image.

Though we have cases for a variety of sources, primary focus centers on those cases associated with easterly waves. Therefore, individual case studies are presented in subsequent subsections for Isabel (2003) and Debby (2000). These cases are chosen due to the ability of our detection technique to track the tropical disturbances associated with these tropical cyclones back to the coast of Africa where they originate as easterly waves.

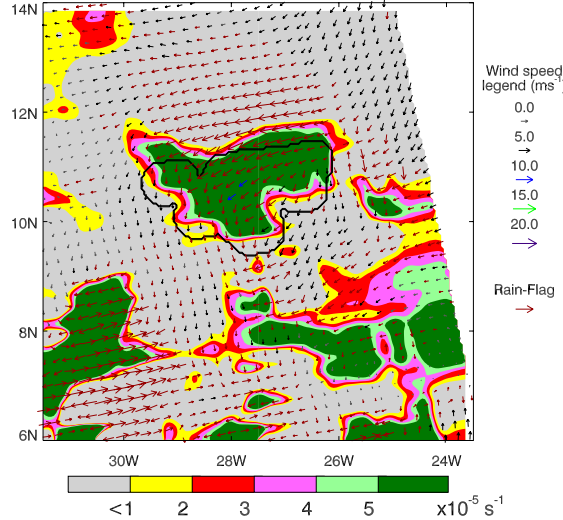
The transition from an easterly wave to tropical cyclone is clearly evident in the pre-TC tracks of the easterly wave cases. This evolution is depicted through comparison of the wind and rain signatures in the areas where the detection technique's criteria are fulfilled within 175 km from the point of convection. Based upon the relationship between the wind and rain signatures, the evolution is subdivided into stages (section 6).

QSCAT Vorticity 1953 UTC 5 September 1999



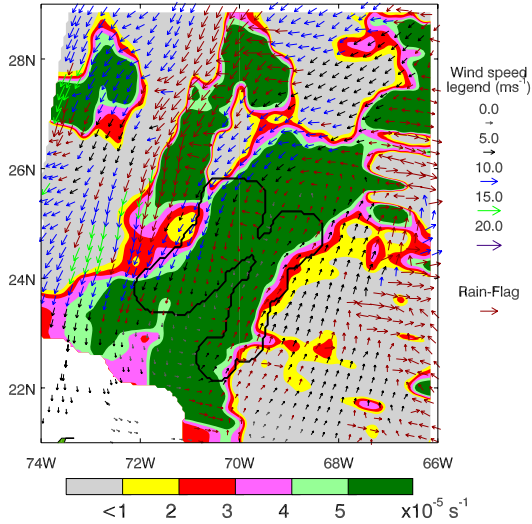
(a)

QSCAT Vorticity 0758 UTC 10 October 2003



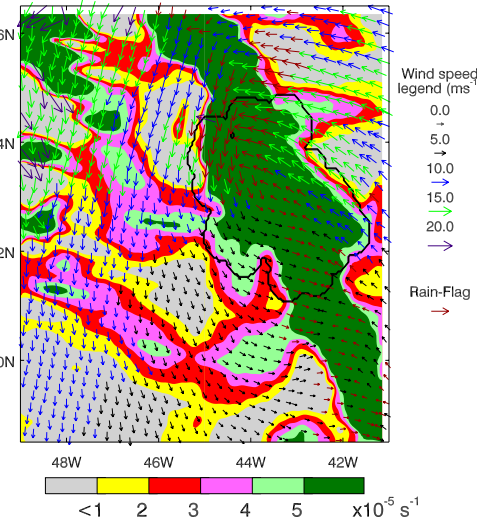
(b)

QSCAT Vorticity 2228 UTC 13 October 2000



(c)

QSCAT Vorticity 2132 UTC 2 November 2001



(d)

Figure 3: Examples of the early stages of TCG that are identified by the vorticity-based detection technique. (a) Floyd, 46 hours before classification as a tropical depression. The vorticity signature shown is associated with the easterly wave that spawned Floyd. (b) Nicholas, 64 hours before classification as a tropical depression. The vorticity signature shown is associated with the easterly wave that produced Nicholas. (c) Michael, 38 hours before classification as a subtropical depression. The vorticity signature shown is associated with the upper-level cold low that interacted with a stationary front to create Michael. (d) Noel, 26 hours before classification as a subtropical storm. The vorticity signature shown is associated with the non-tropical occluded low that spawned Noel. Each example illustrates an apparent surface circulation.

5.1 Isabel (2003)

On 1 September at 1856 UTC, an initial vorticity signature associated with the easterly wave that spawns tropical cyclone Isabel is identified off the coast of Africa (Figures 4a, 5a). The wave continues to progress westward over the next several days and gradually becomes more organized (Figures 4b-d). Vorticity signatures associated with the wave become more consolidated and the surrounding wind pattern begins a counterclockwise rotation (Figures 5b-d). At 1918 UTC 4 September, an apparent weak surface circulation is exhibited in the vorticity signature, with several winds of $10-15\text{ ms}^{-1}$ to the south (Figure 5e). Such a circulation is not clearly evident in the associated GOES infrared image, which is still broad and disorganized (Figure 4e). On 5 September the surface circulation is stronger and more pronounced, with numerous winds of $10-15\text{ ms}^{-1}$ to the north (Figures 5f, g). GOES infrared images, at these same times, also exhibit cyclonic circulation, as well as organized convection (Figures 4f, g). As a result of this adequate organized convection, satellite-based Dvorak estimates begin at 0000 UTC 5 September (Beven and Cobb 2003). At 0000 UTC 6 September, the NHC classifies the tropical disturbance as a tropical depression (Beven and Cobb 2003). This track is illustrated in Figure 6, where the triangles represent the associated QuikSCAT vorticity images, and the number above or below each triangle signify the tracking time for that image.

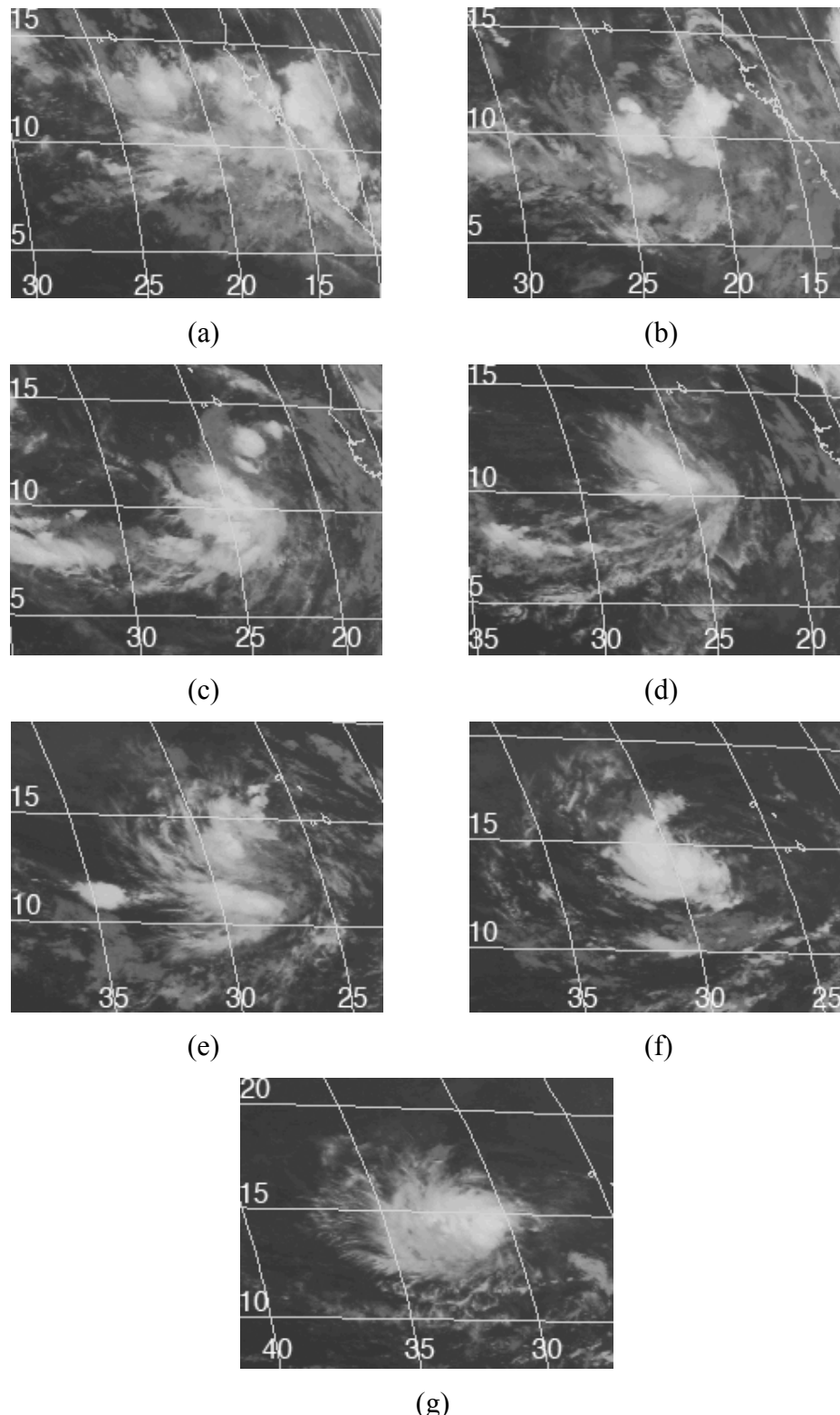
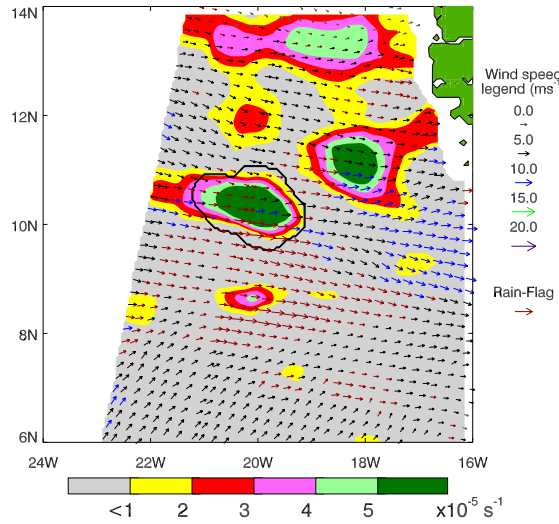


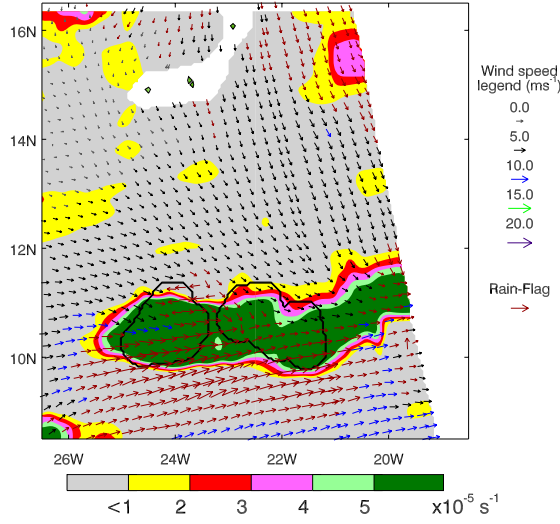
Figure 4: GOES infrared images associated with pre-TC Isabel (2003) for (a) 1 September at 1745 UTC, (b) 2 September at 845 UTC, (c) 3 September at 845 UTC, (d) 3 September at 2045 UTC, (e) 4 September at 2045 UTC, (f) 5 September at 845 UTC, and (g) 5 September at 2045 UTC (courtesy NOAA/NESDIS/CLASS: www.class.noaa.gov).

QSCAT Vorticity 1856 UTC 1 September 2003



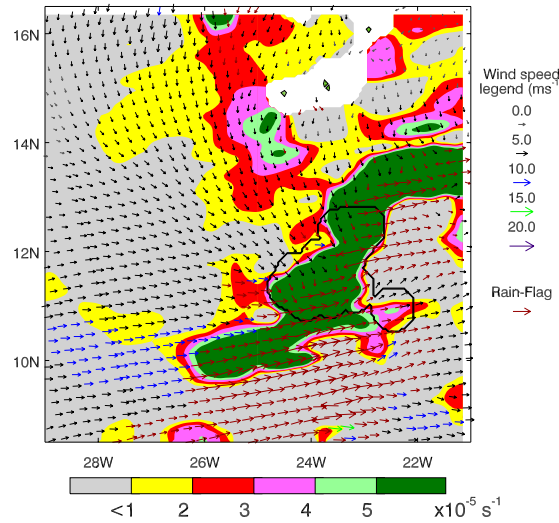
(a)

QSCAT Vorticity 0739 UTC 2 September 2003



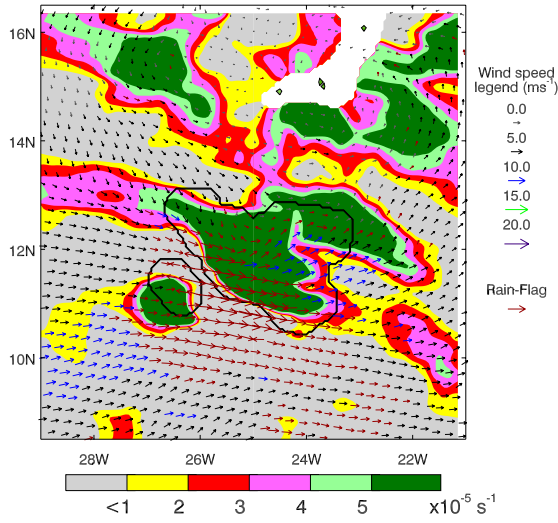
(b)

QSCAT Vorticity 0714 UTC 3 September 2003



(c)

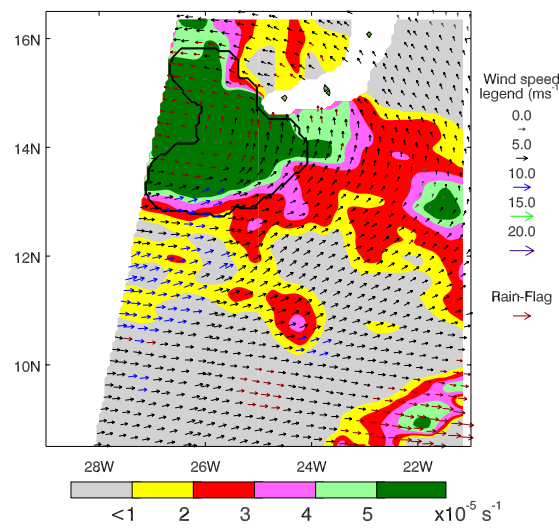
QSCAT Vorticity 1944 UTC 3 September 2003



(d)

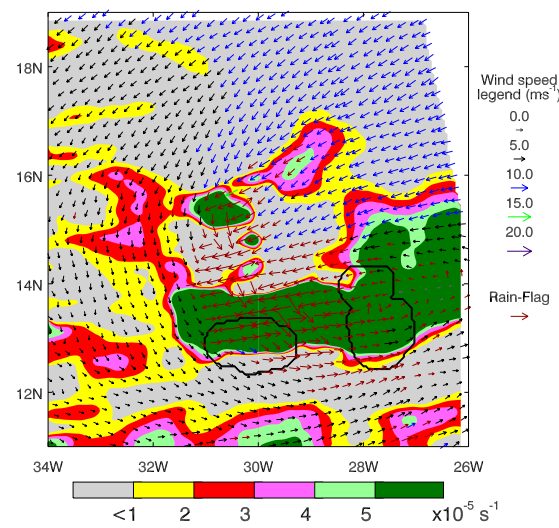
Figure 5: QuikSCAT vorticity images associated with pre-TC Isabel (2003) and the corresponding tracking times. (a) 1 September at 1856 UTC, 101 hours. (b) 2 September at 0739 UTC, 88 hours. (c) 3 September at 0714 UTC, 65 hours. (d) 3 September at 1944 UTC, 52 hours. (e) 4 September at 1918 UTC, 29 hours. (f) 5 September at 0803 UTC, 16 hours. (g) 5 September at 2032 UTC, 3 hours.

QSCAT Vorticity 1918 UTC 4 September 2003



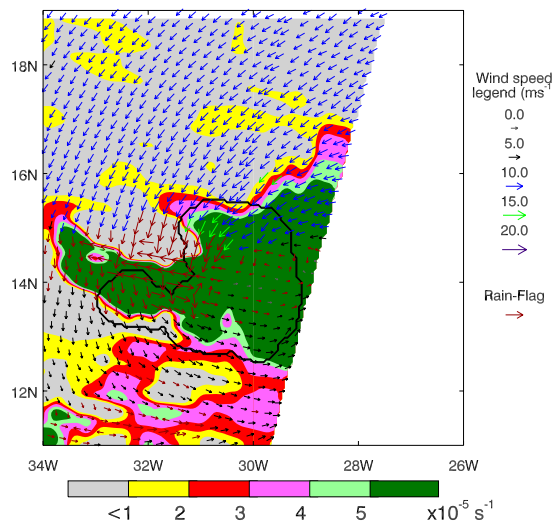
(e)

QSCAT Vorticity 0803 UTC 5 September 2003



(f)

QSCAT Vorticity 2032 UTC 5 September 2003



(g)

Figure 5 cont.

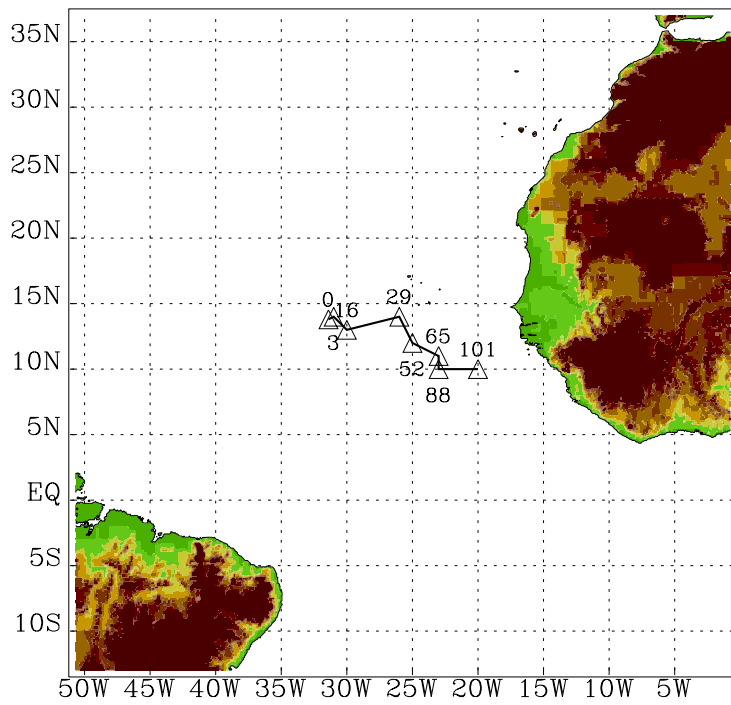


Figure 6: Track of the tropical disturbance associated with pre-TC Isabel (2003). Triangles represent the associated QuikSCAT images, and the number above or below each triangle signify the tracking time for that image. The number ‘0’ represents when the NHC classified Isabel as a tropical depression.

5.2 Debby (2000)

Debby develops from a strong African easterly wave (Pasch 2000). An initial vorticity signature associated with this wave is observed at 1859 UTC 15 August (Figures 7a, 8a). As the wave propagates westward, the surrounding winds gradually begin a cyclonic circulation and a weak surface circulation develops on 17 August (Figures 7b-d, 8b-d). The Tropical Analysis and Forecast Branch (TAFB) observe this broad area of low pressure and are unable to give the disturbance Dvorak classification since there is insufficient curvature in the associated bands of deep convection (Pasch 2000). Therefore, the system is characterized as “too weak to classify” and is monitored (Pasch 2000). Through 18 August the surface circulation continues to become more organized, illustrating a tighter cyclonic rotation and wind speeds of $5-15 \text{ ms}^{-1}$ (Figures 8e, f). Such characteristics are not as evident in the associated GOES infrared images, which still show the disturbance as broad and poorly organized (Figures 7e, f). Instead, the cloud patterns exemplify an increase in curvature among the convective bands, which prompts initial classification of the disturbance by the TAFB at 1145 UTC 18 August (Pasch 2000). The disturbance continues to track westward at approximately 10 ms^{-1} , becoming more organized (Figures 7g, 8g). Approximately 900 nautical miles east of the Windward Islands the cloud pattern associated with the disturbance becomes consolidated around a well-defined center and is categorized by the NHC as a tropical depression on 19 August at 1800 UTC (Pasch 2000). This track is illustrated in Figure 9.

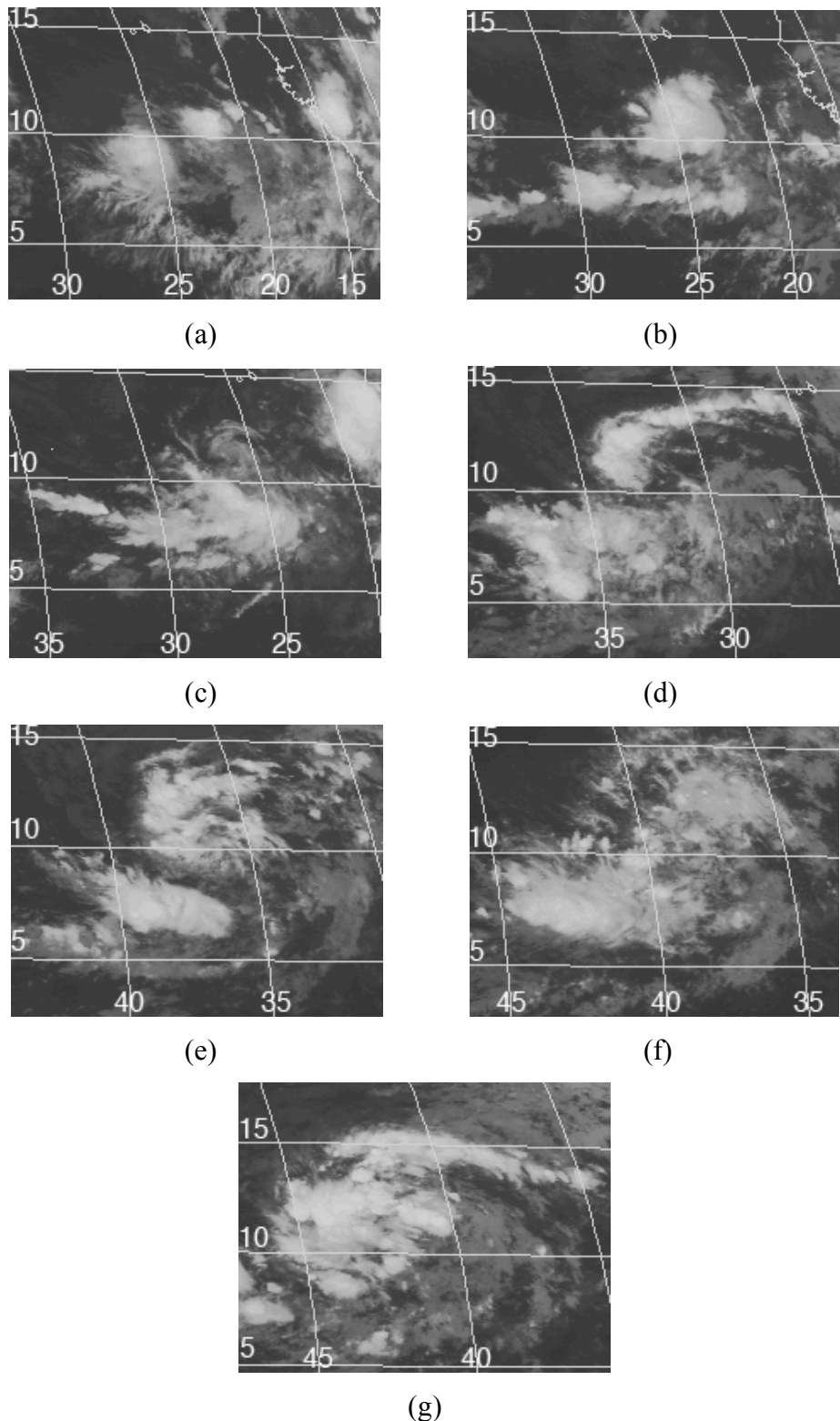


Figure 7: GOES infrared images associated with pre-TC Debby (2000) for (a) 15 August at 2045 UTC, (b) 16 August at 845 UTC, (c) 16 August at 2045 UTC, (d) 17 August at 2045 UTC, (e) 18 August at 845 UTC, (f) 18 August at 2045 UTC, and (g) 19 August at 845 UTC (courtesy NOAA/NESDIS/CLASS).

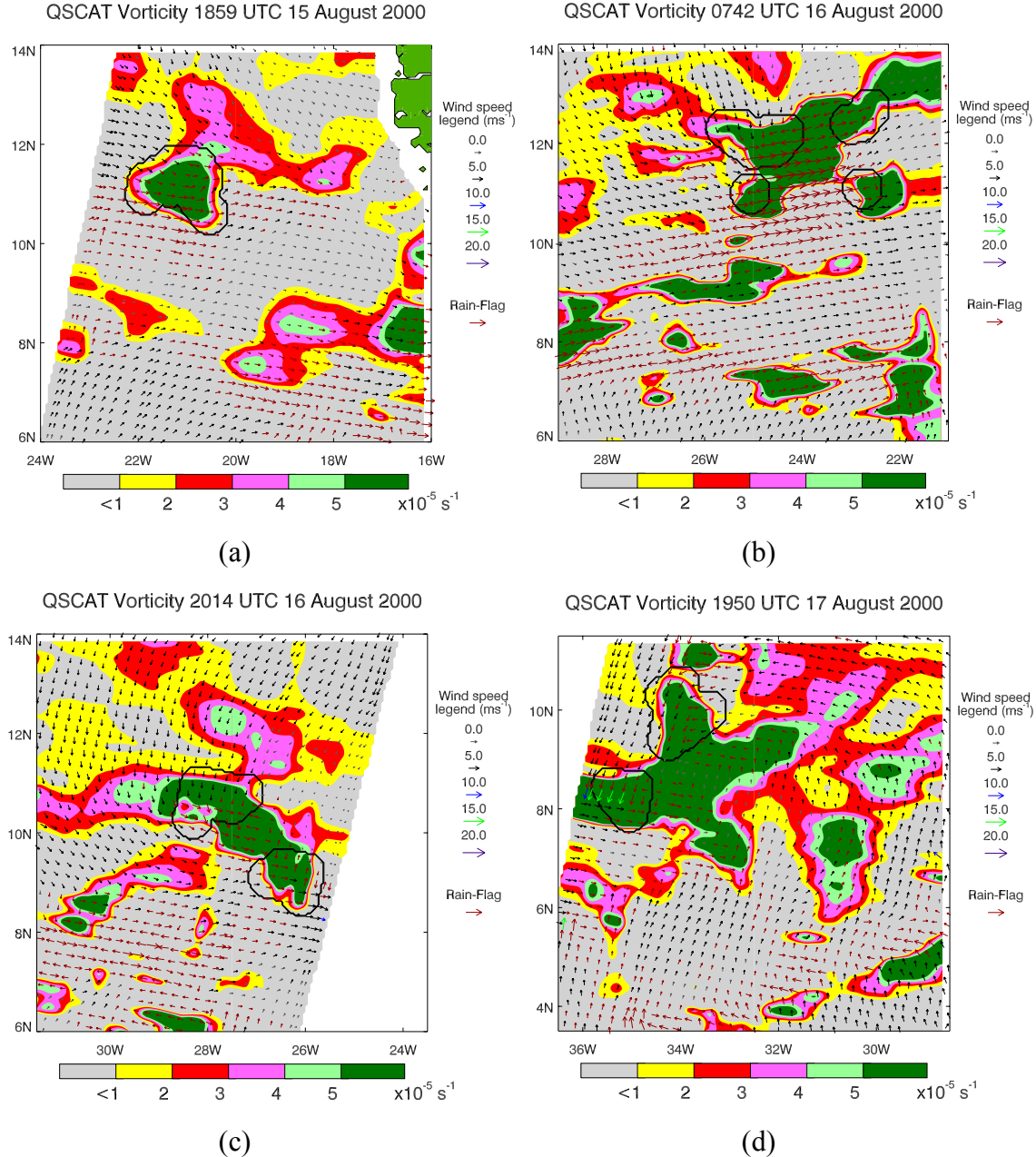
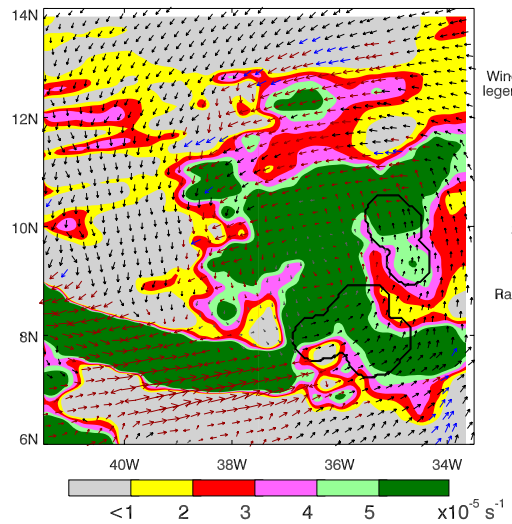


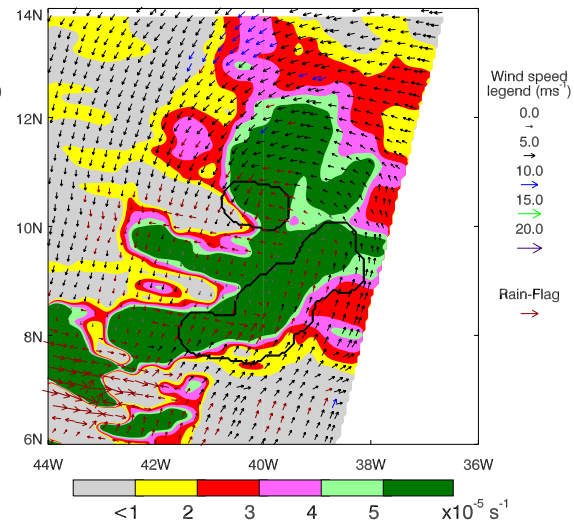
Figure 8: QuikSCAT vorticity images associated with pre-TC Debby (2000) and the corresponding tracking times. (a) 15 August at 1859 UTC, 95 hours. (b) 16 August at 0742 UTC, 82 hours. (c) 16 August at 2014 UTC, 70 hours. (d) 17 August at 1950 UTC, 46 hours. (e) 18 August at 833 UTC, 33 hours. (f) 18 August at 2104 UTC, 21 hours. (g) 19 August at 808 UTC, 10 hours.

QSCAT Vorticity 0833 UTC 18 August 2000



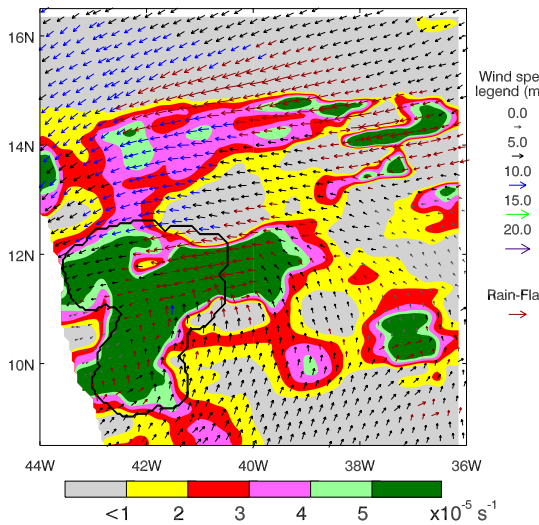
(e)

QSCAT Vorticity 2104 UTC 18 August 2000



(f)

QSCAT Vorticity 0808 UTC 19 August 2000



(g)

Figure 8 cont.

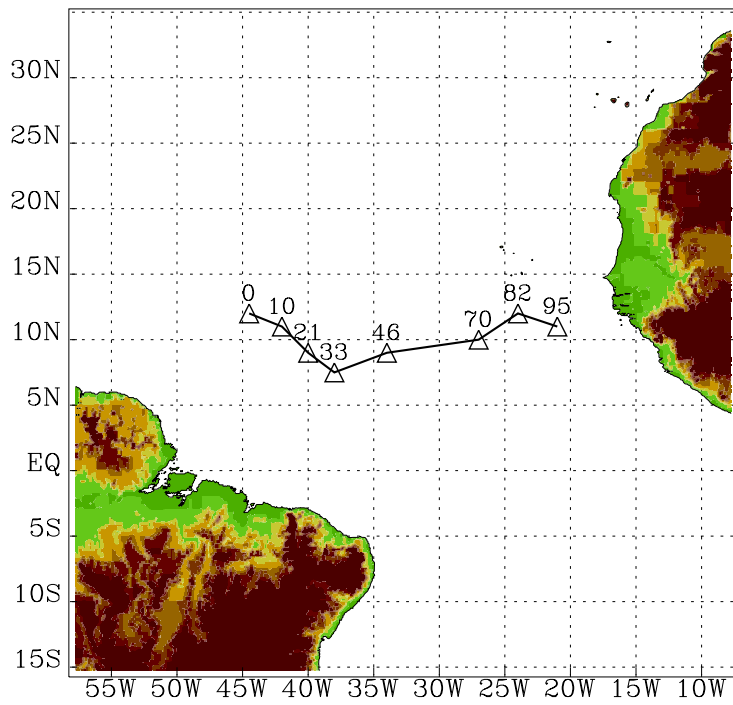


Figure 9: Track of the tropical disturbance associated with pre-TC Debby (2000). Triangles represent the associated QuikSCAT images, and the number above each triangle signifies the tracking time for that image. The number ‘0’ represents when the NHC classified Debby as a tropical depression.

6. DISCUSSIONS

Results from the vorticity-based detection technique prove very effective in identification of tropical disturbances; however, the principal concern with this technique regards the ambiguity removal errors associated with rain-flagged data. These selection errors are evident for the majority of the 15 cases, but the cases more seriously affected are those originating in the tropics (i.e., easterly waves). Disturbances connected with this origin exhibit lower wind speeds and high moisture content, contributing to the significant number of rain flags and, hence, ambiguity removal errors. In contrast, cases that develop from sources other than tropical waves, such as upper-level cut-off lows and stagnant frontal zones, are generally unaffected by the negative influences of rain (i.e., selection errors). Systems associated with such sources have subtropical origins and therefore exhibit higher wind speeds and reduced moisture content. A key example of a subtropical system that illustrates such features is the disturbance associated with pre-TC Noel on November 2 (Figure 3d).

Incorporation of these selection errors within the technique significantly impacts the vorticity calculation. As previously mentioned, average vorticity is calculated within a 100 km by 100 km area using individual vorticity values, which are determined from wind observations at the center of each grid cell via the circulation theorem (section 4.1). Therefore, if the wind observations used to calculate vorticity at each grid cell include ambiguity removal errors on the outer bounds of the averaging box, then the average vorticity is affected. The location where ambiguity errors influence the averaged vorticity is approximately 100 to 140 km from the selection errors.

Cases associated with easterly waves can be considerably affected by the ambiguity selection errors associated with rain-flagged data. Results from the case studies in section 5 demonstrate this problem. The rain-related issues in these two case studies vary throughout the QuikSCAT vorticity-based track; however, a similar vorticity signal-to-noise pattern is evident through comparison of the wind and rain signatures (associated with vorticity signatures that met the detection technique's criteria within 175 km from the center point of convection). The relationship between these signals (i.e.,

wind speed and rain) has been characterized (Weissman et al. 2002; Draper and Long 2004).

The amount of backscattered power that is received by the scatterometer is a function of wind speed and rain characteristics (Weissman et al. 2002). If the wind signal is larger than that of the rain signal, then rain insignificantly affects the backscatter signal. However, if the rain signal is larger than that of the wind signal, then rain influences the backscattered power. The influence of rain distorts the scatterometer signal, potentially creating wind direction reversals in the data which affect the average vorticity calculation. In areas strongly dominated by rain, the scatterometer directions are perpendicular to the nadir track.

Based upon the relationship between wind and rain signatures in the areas where the detection technique's criteria are met (within 175 km from the point of convection), the pre-TC tracks of each easterly wave case are subdivided into stages. These stages consist of an initial, intermediate, and near-TC phase. The initial stage corresponds to the earliest vorticity signatures identified by the detection technique, the near-TC stage is associated with the vorticity signatures detected directly prior to NHC classification, and the intermediate stage constitutes the vorticity signatures between the initial and near-TC stages. Each of these phases is discussed in detail in subsequent sections (sections 6.1-6.3). These stages depict the transition from an easterly wave to tropical cyclone and are further discussed in section 6.4.

6.1 The Initial Stage

In the initial stage there is a lack of closed circulations that can be resolved with 25 km wind vector observations. The vorticity signatures that are identified by the detection technique are small in spatial extent and very weak. Examples of these diminutive, weak signatures are illustrated in Figures 5a and 8a. As seen in these images, the initial vorticity signatures correspond with rain-flagged wind vectors and few large ambiguity removal errors (i.e., wind direction reversals). This situation implies that the wind signal is larger than the rain signal (Weissman et al. 2002). Therefore, any vorticity

modification that occurs as a result of selection errors is small when compared to the signal.

6.2 The Intermediate Stage

Relative to the initial stage, the vorticity signatures identified in the intermediate stage are stronger and have a larger spatial size (Figures 5b-d, 8b-c). The areas where the detection technique's criteria are fulfilled (black solid contours) are inundated with numerous rain-flagged wind vectors and ambiguity removal errors, implying that the vertically integrated rain rates have increased relative to the initial stage. The rain-flagged wind vectors are comparatively large in magnitude and exhibit an across swath direction, signifying rain contamination. This situation implies that the rain signal has grown to dominate the wind signal (Weissman et al. 2002). Medium to strong tropical storms also have this characteristic. Thus, rain-related vorticity modification is equivalent or large when compared to the signal. In these instances, several of the detected location areas appear to be a result of ambiguity selection errors (Figures 5b-d, 8b-c). For example, the QuikSCAT vorticity image associated with pre-TC Isabel at 1944 UTC 3 September 2003 depicts a large and small location area (Figure 5d). The larger position area is accurate, depicting a pseudo circulation pattern; whereas, the smaller location area is a byproduct of selection errors. In regards to this stage, the detection technique is pinning down the general area of the tropical disturbance and, though some identified signatures are byproducts of selection errors, the detection technique is effective. In general, the intermediate stage is the development phase of the pre-TC tracks. Reasoning behind this stems from the beginning of a cyclonic circulation in the surrounding wind pattern and increase of vertically integrated rain rates.

6.3 The Near-TC Stage

Vorticity signatures associated with the near-TC stage are approximately one to two days prior to NHC classification. These signatures are very organized and have a large spatial size (Figures 5e-g, 8d-g). A large-scale cyclonic circulation is present for

each signature with strong wind speeds (strong in relation to the wind speeds in the initial and intermediate stages). The near-TC vorticity signatures correspond with rain-flagged wind vectors and few ambiguity removal errors. This situation implies the wind signal dominates the rain signal (Weissman et al. 2002). Therefore, any vorticity modification that occurs as a result of selection errors is small when compared to the signal. Relative to the intermediate stage, the near-TC stage, with less rain-related problems, indicates that either the rain rate has been reduced (which we have not examined) or that the wind speeds have increased. The latter of which is clearly true.

6.4 Pre-TC Track Transition

The vorticity signal-to-noise pattern associated with the QuikSCAT vorticity-based tracks of the two individual case studies clearly depict the transition from an easterly wave to tropical cyclone and the phases associated with this transition (initial, intermediate, and near-TC stage). The initial stage is associated with very weak vorticity signatures that have small spatial scales. These initial signals are often related to horizontal shear embedded in eastward winds and are insignificantly affected by rain. The intermediate stage constitutes vorticity signatures that are greatly influenced by rain and rain-related problems, as well as the beginning of a large-scale cyclonic circulation. The intermediate stage is of significant importance to the evolution of an easterly wave to tropical cyclone since it represents a development stage, where stronger precipitation can lead to increased cyclonic circulation. As a result of this growth, the vorticity signatures corresponding to the near-TC stage are highly organized, with large spatial sizes, increased wind speeds, and large-scale cyclonic circulations. The surface signatures of these tropical disturbances, as well as the cloud pattern, continue to strengthen and organize.

6.5 Future Improvements

Improvements in scatterometer design, as well as wind retrieval algorithms, could be improved upon to better account for rain. The SeaWinds scatterometer uses the Ku-

band and large incidence angles, both of which result in more sensitivity to rain. The point-wise wind retrieval method is also substantially affected by rain. However, if the incidence angles are reduced and a different frequency (e.g., C-band) or combination of frequencies (e.g., Ku and C-band) is used, then rain would be less of an issue. The use of a field-wise wind retrieval method would also prove beneficial, reducing rain-related problems (i.e., ambiguity removal errors). Unlike point-wise wind retrieval, which calculates the wind at each WVC individually, field-wise wind retrieval determines the wind for an entire region of WVCs, acknowledging that a correlation exists between each wind vector in a field of cells. Overall, the addition of a radiometer (e.g., AMSR) on the same platform as the SeaWinds scatterometer would greatly improve rain-impact flags and rain corrections.

7. CONCLUSIONS

A vorticity-based detection technique is developed to identify and monitor tropical disturbances associated with the early stages of TCG in the Atlantic basin. Detection is based on visual inspection of GOES infrared images, as well as surface structure. From a sampling of 15 tropical cyclones during the 1999-2004 Atlantic hurricane seasons the technique identifies tropical disturbances approximately 19 to 101 hours before classification by the NHC. Herein the minimum tracking time is associated with pre-TC Karen (2001); whereas, the maximum tracking time is associated with pre-TC Jerry (2001) and pre-TC Isabel (2003). Smaller tracking times are associated with systems that develop from sources other than easterly waves, such as upper-level cut-off lows and stagnant frontal zones. The shorter tracking times stem from land interference, which QuikSCAT lacks the ability to resolve since it only provides observations over water. Larger tracking times correspond to cases that originate from African easterly waves. Focus is primarily concentrated on such cases, due to approximately 63% of all Atlantic tropical cyclones being associated with tropical waves.

Overall results for the 15 cases prove very successful. Therefore, the vorticity-based detection technique described herein is an effective tool in identifying and monitoring tropical disturbances in the genesis stage. For easterly wave cases, the detection technique has the ability to track tropical disturbances from near the coast of Africa. The pre-TC tracks of these cases depict the evolution of an easterly wave to tropical cyclone and stages associated with this transition. These stages consist of an initial, intermediate, and near-TC phase, which are related to spatial extent, wind speed, and precipitation characteristics. Though there is room for improvements regarding scatterometer design and wind retrieval algorithms to better account for the influences of rain, it is reasonable to assume that this technique could be useful to scientific and operational communities.

REFERENCES

- Avila, L. A., and R. Pasch, 1992: Atlantic tropical systems of 1991. *Mon. Wea. Rev.*, **120**, 2696-2699.
- Avila, L. A., and E. N. Rappaport, 1996: Atlantic hurricane season of 1994. *Mon. Wea. Rev.*, **124**, 1558-1578.
- Beven, J., and H. Cobb, 2003: Tropical cyclone report hurricane Isabel 6-19 September 2003. NCEP Rep., 24 pp. [Available online at www.nhc.noaa.gov/2003isabel.shtml?.]
- Bister, M., and K. A. Emanuel, 1997: The genesis of Hurricane Guillermo: TEMEX analyses and a modeling study. *Mon. Wea. Rev.*, **125**, 2662-2682.
- Bliven, L. F., H. Branger, P. W. Sobieski, and J. P. Giovanageli, 1993: An analysis of scatterometer returns from a water agitated by artificial rain. *Int. J. Remote Sens.*, **14**, 2315-2329.
- Bosart, L. F., and F. Sanders, 1981: The Johnstown flood of July 1977: A long-lived convective system. *J. Atmos. Sci.*, **119**, 1979-2013.
- Bourassa, M. A., D. M. Legler, and J. J. O'Brien, 2003: Scatterometry data sets: High quality winds over water. *Advances in the Applications of Marine Climatology – The Dynamic Part of the WMO Guide to the Applications of Marine Climatology*. JCOMM Technical Report No. 13 WMO/TD-No.1081, 159-174.
- Bracken, W. E., and L. F. Bosart, 2000: The role of synoptic scale flow during tropical cyclogenesis over the North Atlantic Ocean. *Mon. Wea. Rev.*, **128**, 353-376.
- Burpee, R. W., 1972: The origin and structure of easterly waves in the lower troposphere in North Africa. *J. Atmos. Sci.*, **29**, 77-90.
- Burpee, R. W., 1974: Characteristics of North African easterly waves during the summers of 1968 and 1969. *J. Atmos. Sci.*, **31**, 1556-1570.
- Burpee, R. W., 1975: Some features of synoptic-scale waves based on compositing analysis of GATE data. *Mon. Wea. Rev.*, **103**, 921-925.
- Carlson, T. N., 1969: Synoptic histories of three African wave disturbances that developed into Atlantic hurricanes. *Mon. Wea. Rev.*, **97**, 256-276.
- Davis, C. A., and L. F. Bosart, 2001: Numerical simulations of the genesis of Hurricane Diana (1984). Part I: Control simulation. *Mon. Wea. Rev.*, **129**, 1859-1881.

- Donelan, M. A., and W. J. Pierson, 1987: Radar scattering and equilibrium ranges in wind generated waves with application to scatterometry. *J. Geophys. Res.*, **92**, 4971–5029.
- Draper, D. W., and D. G. Long, 2004: Simultaneous wind and rain retrieval using SeaWinds data. *IEEE Trans. Geosci. Remote Sens.*, **42**, 1411-1423.
- Frank, W. M., 1988: Tropical cyclone formation. *A Global View of Tropical Cyclones*, R. L. Elsberry, Ed., 53-90.
- Katsaros, K. B., E. B. Forde, P. Chang, and W. T. Liu, 2001: QuikSCAT's SeaWinds facilitates early identification of tropical depressions in 1999 hurricane season. *Geophys. Res. Lett.*, **28**, 1043-1046.
- Liu, W. T., 2001: Wind over troubled water. *Backscatter*, **12**, 10-14.
- Montgomery, M. T., and J. Enagonio, 1998: Tropical cyclogenesis via convectively forced vortex Rossby waves in a three-dimensional quasigeostrophic model. *J. Atmos. Sci.*, **55**, 3176-3207.
- Naderi, F. M., M. H. Freilich, and D. G. Long, 1991: Spaceborne radar measurements of wind velocity over the ocean-An overview of the NSCAT scatterometer system. *Proc. IEEE*, **79**, 850-866.
- Pasch, R. J., 2000: Tropical cyclone report hurricane Debby 19-24 August 2000. NCEP Rep., 10 pp. [Available online at www.nhc.noaa.gov/2000debby.html.]
- Reed, R. J., D. C. Norquist, and E. E. Recker, 1977: The structure and properties of African wave disturbances as observed during Phase III of GATE. *Mon. Wea. Rev.*, **105**, 317-333.
- Richards, S. L., 1999: A field-wise retrieval algorithm for SeaWinds. M.S. thesis, Dept. of Electrical and Computer Engineering, Brigham Young University, 148 pp.
- Riehl, H., 1954: *Tropical Meteorology*. McGraw-Hill, 392 pp.
- Riehl, H., 1979: *Climate and Weather in the Tropics*. Academic Press, 611 pp.
- Ritchie, E. A., and G. H. Holland, 1997: Scale interactions during the formation of Typhoon Irving. *Mon. Wea. Rev.*, **125**, 1377-1396.
- Shaffer, S. J., R. S. Dunbar, S. V. Hsiao, and D. G. Long, 1991: A median-filter-based ambiguity removal algorithm for NSCAT. *IEEE Trans. Geosci. Remote Sens.*, **29**, 167-174.

- Sharp, R. J., M. A. Bourassa, and J. J. O'Brien, 2002: Early detection of tropical cyclones using SeaWinds-derived vorticity. *Bull. Amer. Meteor. Soc.*, **83**, 879-889.
- Simpson, J., E. Ritchie, G. J. Holland, J. Halverson, and S. Stewart, 1997: Mesoscale interactions in tropical cyclone genesis. *Mon. Wea. Rev.*, **125**, 2643-2661.
- Sobieski, P., and L. F. Bliven, 1995: Analysis of high speed images of raindrop splash products and Ku-band scatterometer returns. *Int. J. Remote Sens.*, **16**, 2721-2726.
- Sobieski, P., C. Craeye, and L. F. Bliven, 1999: Scatterometric signatures of multivariate drop impacts on fresh and salt water surfaces. *Int. J. Remote Sens.*, **20**, 2149-2166.
- Thorncroft, C. D., and B. J. Hoskins, 1994a: An idealized study of African easterly waves. Part I: A linear view. *Quart. J. Roy. Meteor. Soc.*, **120**, 953-982.
- Thorncroft, C. D., and B. J. Hoskins, 1994b: An idealized study of African easterly waves. Part II: A nonlinear view. *Quart. J. Roy. Meteor. Soc.*, **120**, 983-1015.
- Weissman, D. E., M. A. Bourassa, and J. Tongue, 2002: Effects of rain rate and wind magnitude on SeaWinds scatterometer wind speed errors. *J. Atmos. Oceanic Technol.*, **19**, 738-746.
- Weissman, D. E., M. A. Bourassa, J. Tongue, and J. J. O'Brien, 2003: Calibrating the QuikSCAT/SeaWinds radar for measuring rain over water. *IEEE Trans. Geosci. Remote Sens.*, **41**, 2814-2820.
- Wentz, F. J., and D. K. Smith, 1999: A model function for the ocean-normalized radar cross section at 14 GHz derived from NSCAT observations. *J. Geophys. Res.*, **104**, 11 499-11 514.
- Wentz, F. J., D. K. Smith, C. A. Mears, and C. L. Gentemann, 2001: Advanced algorithms for QuikSCAT and SeaWinds/AMSR. *Geosci. Remote Sen. Symposium, 2001. IGARSS'01. IEEE 2001 International*, **3**, 1079-1081.

BIOGRAPHICAL SKETCH

Education

M.S. Meteorology, April 2006, The Florida State University, Tallahassee, Florida

B.S. Meteorology, April 2004, The Florida State University, Tallahassee, Florida

Experience

Fall 2004 - present: Graduate Research Assistant / COAPS*, FSU

Spring - Summer 2004: Undergraduate Research Assistant / COAPS*, FSU

Fall 2003 - Spring 2004: Teaching Assistant / Department of Meteorology, FSU

* Center for Ocean-Atmospheric Prediction Studies

Memberships

American Meteorological Society

Chi Epsilon Pi - Meteorological Honor Society